ADVANCED MATERIALS TECHNOLOGIES
www.advmattechnol.de

Dynamically Conformal Mask Printing of Liquid Alloy Circuits on Morphing Objects

*Shuo Zhang, Jiajun Jiang, Qin Jiang, Wenjie Fei, Chuan Fei Guo, and Zhigang Wu**

Due to their excellent conformability and inherent compatibility, soft three-dimensional (3D) circuits can promisingly contribute to soft intelligent systems, i.e., soft robots equipped with dynamic and sophisticated morphologies. However, current processing technologies have almost focused on fabricating planar or 3D circuits on static objects, which restrict the feasibility when targeting on dynamic/morphing surfaces in case of mismatched stress or strain. Here, a conformal mask printing method, based on selective laser patterninga conformal, attachable and dynamic (CAD) film made of carbon black-doped polydimethylsiloxane (cPDMS) is reported. Combining with the unique fluidity of liquid alloy, the new CAD-mask allows to conformably print dynamic compliant liquid alloy circuits on various complex and morphing surfaces. To illustrate the capability of the approach, 3D conformal circuits are fabricated on a steering wheel for detecting driving modes, on a face model to achieve anthropomorphic layer, and demonstrate the fabrication process on adynamic shape-changing elastomeric heart and a human hand. The approach offers a new opportunity for real-timely configuring dynamic compliant circuits on morphing substrates of soft electronics/robotics.

1. Introduction

Soft/flexible electronics have been promisingly applied to wearable devices,[1] medical equipment,[2] and soft robotics,[3] due to its mechanical and electrical reliability, excellent compliance, and rich functionality inherited from intrinsically stretchable materials or subtle designs.[4] To achieve reliable functionalities in diverse applications, many methods have been developed for fabricating flexible/soft and robust circuits on planar or deployed and regular 3D surfaces,[5] such as transfer printing[6] and 3D printing.[7] However, traditional planar transfer printing employed metal foil circuits with serpentine or hierarchical structures to integrate on 3D surfaces with continuous curvatures,[6b,8] usually the delamination would be a potential issue under out-of-plane deformation or large elongation because of mechanical mismatch. Alternative solution, 3D printing, is potential for fabricating circuits on arbitrary surfaces with precise designs. Nevertheless, it usually requires modified inks and specific instrument,[7b,c,9] which is not always technique-ready for various objects with complex surfaces. Of particular, when interacting with morphing objects such as human with kinetic movements and morphing epidermis, and robots with changeable shapes or dynamic morphologies, these methods still have challenges on matching with target substrates, especially the growing or continuously deforming ones, with good conformability and robustness.

Recently, morphing electronics has been proposed to adapt to in vivo nerve growth with minimal mechanical constraint.[10] Apart from solid metal foil circuits, Gallium-based liquid alloy, e.g. Galinstan or EGaIn, was widely employed for fabricating stretchable electronics because of its unique fluidity, inherent stretchability, and strong adhesion of the oxide layer on diverse surfaces.[11] Many approaches such as capillary filling,[12] direct writing,[13] contact printing,[14] mask printing,[15] atomized printing,[16] 3D printing,[17] flexography printing,[18] and water transfer printing,[19] have also been demonstrated for configuring planar or 3D complex circuits,[20] which were able to adapt to large deformation under harsh conditions. Various printing techniques with high resolution have also been demonstrated over diverse substrates.[21] Further, some recent works have provided successful methods for transferring 2D liquid metal circuits onto 3D shapes. Silver nanoparticles and liquid metal have been reported to be hydroprinted on 3D objects,[22] human body,[23] and even growing plants.[19] High-fidelity circuits on 3D complex can be conformably printed in an automatic way.[18] And mask sprayed printing techniques and related applications have been investigated intensively.[24]

With the development of soft intelligent systems, e.g. wearable system, epidermal electronics and soft/micro robots, and dynamic deployments are becoming indispensable for many applications on human, animal, and even plants. Both the printing process and the printed system are necessary to adapt to dynamic/continuous changeable targets or situations,

S. Zhang, J. Jiang, Q. Jiang, W. Fei, Prof. Z. Wu
State Key Laboratory of Digital Manufacturing Equipment and Technology
School of Mechanical Science and Engineering
Huazhong University of Science and Technology
Wuhan, China
E-mail: zgwu@hust.edu.cn
Prof. C. F. Guo
Department of Materials Science and Engineering
Southern University of Science and Technology
Shenzhen, China
The ORCID identification number(s) for the author(s) of this article can be found under https://doi.org/10.1002/admt.202001274.

DOI: 10.1002/admt.202001274

especially for some animals and organs, e.g. hearts that are always subjected to large deformations in routine. Nevertheless, despite changeable morphs, the aforementioned techniques were still conducted on condition of static objects, which is difficult to be used for continuously varied objects with dynamic morphologies. A method for soft intelligent systems with dynamic and sophisticated morphologies will obviously improve the integrating feasibility.

To deploy electronics onto changeable shapes or dynamic morphologies with good conformability and robustness, the mask should be soft, stretchable, and instant attachable on various surfaces, guaranteeing the conformability and robustness under morphing conditions. However, without being soft, stretchable, and sticky simultaneously, current polymer film and commercial film[15,24b,25] could not be directly applied to such dynamic/morphing objects. Here, we employ an ultrasoft and stretchable carbon black-doped polydimethylsiloxane (cPDMS) (Figure S1, Supporting Information) as a conformal, attachable and dynamic (CAD) mask via laser patterning to real-timely print dynamic liquid alloy circuits on morphing 3D arbitrary surfaces. The ultra-low Young's modulus and elongation of the CAD-mask provide it an excellent conformability and compliance on various 3D complex surfaces. Due to its sticky surface, the CAD-mask shows a robust attachability on dynamic targeting surfaces under continuous deformation with high interfacial adhesion force. Combining with liquid alloy spraying, we demonstrate a liquid alloy circuits-integrated wheel for detecting driving modes and an anthropomorphic social robot for interacting with human. Further, we demonstrate the CAD-mask printing processes on a beating silicone rubber heart and a kinetic human hand for showing the feasibility of fabricating dynamic liquid alloy circuits. The dynamic compliant liquid alloy circuits fabricated by CAD-mask printing provide a potential approach to real-timely configure morphing electronics on arbitrary surfaces regardless of objects' states, contributing to the integration and communication of the internet of things.

2. Results and Discussion

2.1. Design and Fabrication Process of CAD-Mask Printing

As shown in **Figure 1**a, a thin film of cPDMS that laminated on a piece of toner transfer paper (coated with a water-soluble layer) was selectively patterned by an ultraviolet (UV) laser marker. After removing the residual, the CAD-mask was placed on the target surface, here a 3D complex surface of a beating elastomeric heart, and the back side of the toner transfer paper was wetted by water, simultaneously. After being fully wetted by water, the toner transfer paper could be removed, leaving the CAD-mask loosely attached on the target surface. Due to the native stretchability and attachability of cPDMS, the mask could be conformably adhered on the morphing surface by further gentle pressing, Figure 1b. Specifically, during air aerating and pumping, the CAD-mask could be also concurrently inflated and shrunk corresponding to beating process with robust compliance and attachability. Next, by combining with atomized spraying liquid alloy and CAD-mask removing, the liquid alloy circuits were dynamically and seamlessly printed on the surface of the morphing object.

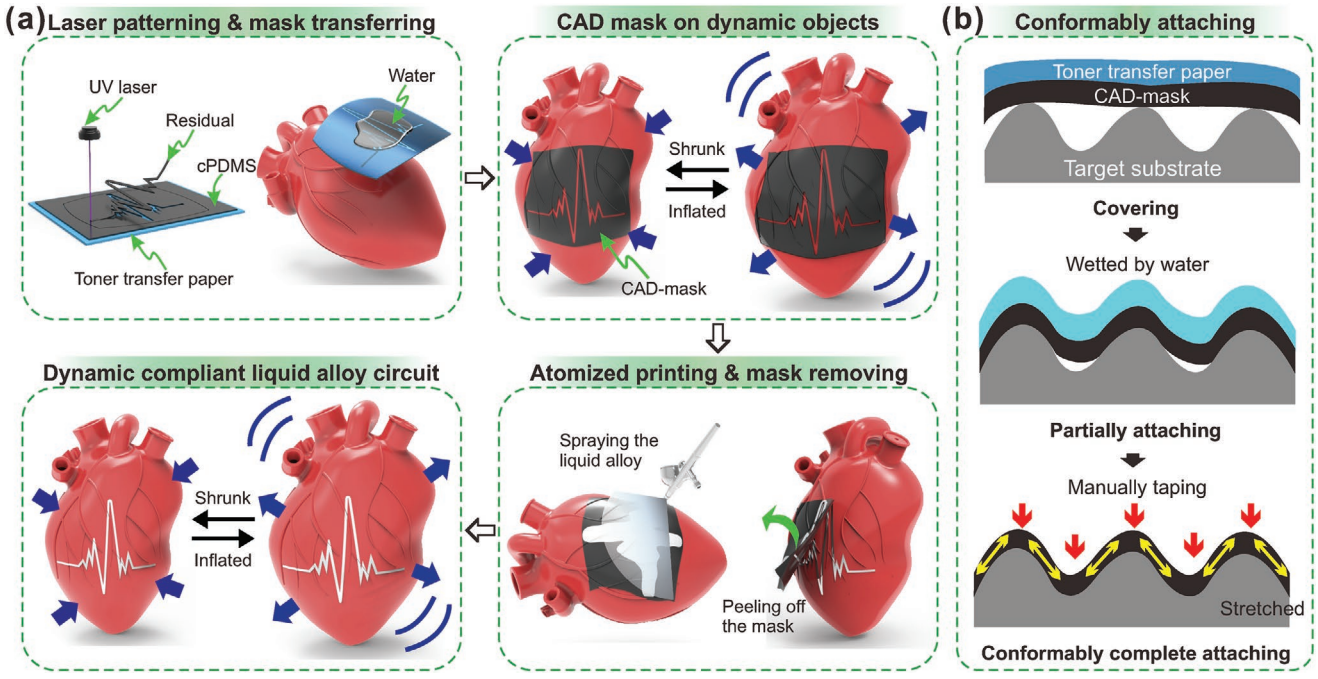

Figure 1. Schematic illustrations of printing dynamic compliant liquid alloy circuits on morphing objects via the conformal, attachable and dynamic (CAD) mask. a) The fabrication process includes ultraviolet (UV)-laser planar mask patterning, mask transferring (onto dynamic 3D surfaces with water soluble substrate), atomized liquid alloy printing, and the conformal mask removing. And finally, the dynamic compliant liquid alloy circuit was attached on the morphing 3D surfaces. b) Detailed schematic illustrations of conformal transferring CAD-mask on target 3D surfaces.

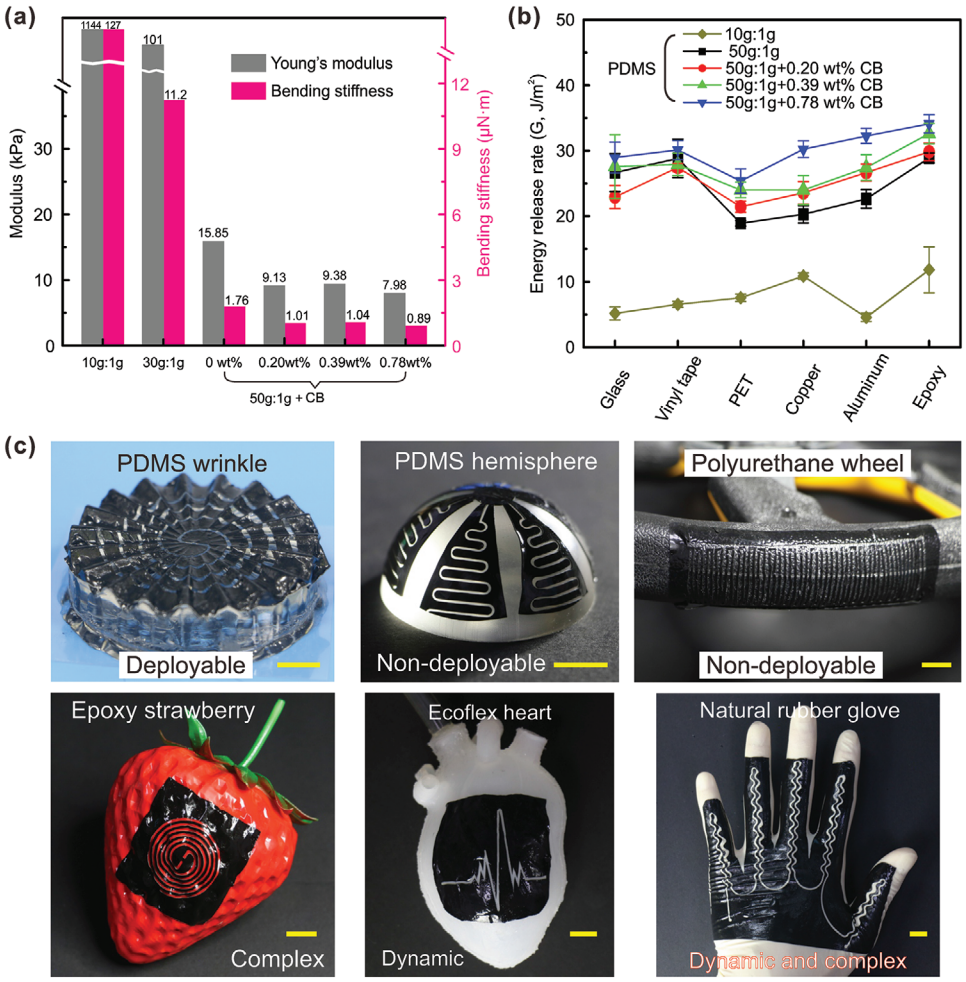

Figure 2. Investigations and demonstrations of the CAD-mask. a) The Young's modulus and bending stiffness of polydimethylsiloxane (PDMS) with 10:1, 30:1, and 50:1 weight ratio, and 50:1 PDMS doped with 0.20, 0.39, and 0.78 wt% of carbon black. b) The energy release rate between the CAD-mask and diverse surfaces. c) The CAD-masks conformably attached on several 3D complex surfaces. The various 3D surfaces of different materials include a complex surface with pits of an epoxy-based strawberry mold, a non-deployable semi-sphere surface of a PDMS mold, a non-deployable of a polyurethane wheel, a deployable wrinkled surface of a PDMS mold, a dynamic 3D surface of a beating Ecoflex heart, and a dynamic and complex 3D surface of a natural rubber. Scale bars = 10 mm.

2.2. Investigation of CAD-Mask

Targeting for 3D complex surfaces of various materials, the flexibility, stretchability, and attachability of the CAD-mask are significant features for the fabrication process. To evaluate the mechanical property of the CAD-mask, we conducted a series tensile tests of PDMS with different cross-linking degrees (10:1, 30:1, and 50:1 weight ratio of silicone base: curing agent), as shown in **Figure 2**a. The Young's modulus and bending stiffness of PDMS with low cross-linking degree (50:1) are both much lower than that of PDMS with high cross-linking degree (10:1 and 30:1), indicating that the PDMS with 50:1 weight ratio is extremely soft to be deformed for matching complex surfaces with different curvatures. Moreover, comparing pure PDMS (50:1) and cPDMS (50:1 PDMS mixed with different weights of carbon black, e.g. 0.1, 0.2, and 0.4), the cPDMS shows a little lower Young's modulus and bending stiffness than that of pure PDMS, which indicates that the doping of carbon black helps to reduce the stiffness of cured PDMS. It may be caused by the lubricity of carbon nanoparticles introduced in PDMS matrix. In addition, the result of tensile test in Figure S2 (Supporting Information) also shows that PDMS/cPDMS with lower cross-linking degree (50:1) possessess high stretchability, indicating a good deformability when needed morphing during conformal printing.

Further, the energy release rate of PDMS on diverse materials' surfaces were conducted with an adhesion test, Figure 2b (detailed measurement setup is illustrated in Figure S3, Supporting Information). As a control group, PDMS with 10:1 weight ratio shows a <6 J m^{-2} energy release rate on surfaces of glass, polyethylene terephthalate (PET), and vinyl tape and aluminum, a >7 J m^{-2} energy release rate on copper and epoxy. For PDMS/cPDMS with 50:1 weight ratio, the energy release rate was much higher than that of the control group. The increased adhesion of PDMS with 50:1 weight ratio was because the lower cross-linking network increased the Van der Waals' force with

better wetting and spreading.[1,26] And with more carbon black doped, the energy release rate force improved. Moreover, the conformability observation in Figure S4 (Supporting Information) convincingly demonstrate the cPDMS with 50:1 weight ratio is proper for conformably attaching the 3D surfaces. These results reveal that cPDMS (50:1-0.1, 0.2, and 0.4, silicone base: curing agent: carbon black, 0.20 wt%, 0.39 wt%, 0.78 wt% carbon black, respectively) has both high flexibility and attachability to conformably match surfaces with different morphologies of diverse materials.

To evaluate the printing versatility of our CAD-mask, we transferred CAD-masks with different patterns on diverse 3D complex surfaces of different materials. As shown in Figure 2c, a CAD-mask with 1 mm width double-helix pattern was conformably attached on a PDMS substrate with deployable wrinkle structures. A krigami-like CAD-mask with serpentine pattern was conformably printed on a nondeployable surface of a PDMS hemisphere substrate. A CAD-mask with sawtooth-like patterns was conformably attached on the nondeployed surface of a polyurethane wheel. And the CAD-mask with double-helix pattern was conformably attached on a complex surface of an epoxy strawberry mould with numbers of sunken pits. Apart from the above static 3D surfaces, the CAD-masks were also dynamically transferred on morphing objects, such as a beating elastomeric heart and a human hand wearing a natural rubber glove. The CAD-mask could not only match the target 3D surface with good compliance, but also shows a superior shape reconfigurability upon the dynamic status of morphing objects.

2.3. Mask Laser Patterning and Printed Liquid Alloy Patterns

The reason of employing carbon black was improving the light absorption of the ultraviolet, to effectively treat the CAD-mask. We observed the profiles of laser-ablated patterns that were obtained under different parameters. As shown in **Figure 3**a, for CAD-masks doped with different weights of carbon black, e.g. 0.1, 0.2, and 0.4 g, the depth and width of laser-ablated channels varied from ≈22 to 30 μm and from ≈45 to 55 μm, respectively. Among them, the CAD-mask doped with 0.2 g carbon black showed the largest depth, even though there was not too much difference between these three samples. In the following work,we employed cPDMS doped with 0.39 wt% carbon black to make CAD-mask. For laser processing times, as shown in Figure 3b, with more treating times, the depth of ablated channel increased, while the width almost maintained as ≈50 μm. It indicates that we can improve the efficiency with more processing times without sacrificing the resolution of width. Figure 3c,d investigated the influence of laser parameters, e.g. scanning speed (v) and pulse repetition frequency (f), on groove's cross profile. When the v was fixed at 100 mm s^{-1}, the maximum depth was ≈150 μm on condition of f = 50 kHz; when the f was fixed at 50 kHz, the maximum depth was also ≈150 μm on condition of v = 100 mm s^{-1}. The maximum depth of channel was obtained at the parameters of v = 100 mm s^{-1} and f = 50 kHz, this might be induced by that the higher the v was, the less time the laser beam took to ablate the specific area, and the less power density to generate. Besides, with the lower v (50 mm s^{-1}), a larger power density was generated, which might result in overablating and particles deposited, as we investigated in previous work.[27] In addition, by changing the f from 30, 70, to 90 kHz, the maximum depth was also obtained under v = 100 mm s^{-1} (Figure S5, Supporting Information). It indicates that the parameter settings of 100 mm s^{-1} and 50 kHz generate the most effective ablation and patterning on CAD-mask.

Moreover, we measured the morphologies and electrical properties of printed liquid alloy traces with different widths. As shown in Figure 3e, the result shows uniform profiles based on designed widths from 25 to 500 μm, while the widths of liquid alloy traces were a little larger than the corresponding designed widths of CAD-mask patterns due to the non-negligible facula and ablation effect of the laser beam (Figure S6, Supporting Information). With increasing of widths, the heights also increased. Of particular, when the designed width was 500 μm, the height reduced to ≈70 μm because of the surface tension of the oxide layer. From Figure 3e, the thickness of sprayed liquid alloy trace was very thin (less than 100 μm) which guaranteed the stability of liquid alloy pinned on dynamic/morphing 3D surface in our demonstration. Further, we measured the resistance of printed liquid alloy lines with different widths on different cambered surfaces (Figures 3f and S7, Supporting Information). The results show diminishing resistance tendencies along increased widths, indicating the electrical reliability and versatility of CAD-mask printed liquid alloy traces. Even though the thickness of sprayed liquid alloy trace could not maintain even due to effect of gravity, the oxide layer and thin thickness played important roles in stable electrical conductivity. Moreover, we also measured the resistance on several pins of printed liquid alloy traces (experimental width of ≈130 μm) (Figure 3g and S8, Supporting Information), and the result shows almost linear trends of three traces, revealing the uniformity of printed liquid alloy. And the variable resistance of liquid alloy lines (experimental widths of ≈50 and ≈150 μm) during stretching–releasing test shows a periodic resilience (Figure 3h). These results suggest a good quality of printed liquid alloy lines.

To demonstrate the applicability of CAD-mask printing, a few conformal liquid alloy circuits were printed on 3D complex surfaces. As shown in **Figure 4**a, the liquid alloy school badge pattern of HUST was printed on the 3D curve surface of a cPDMS substrate with maximum depth of 26.61 mm and maximum curvature of 146.6 m^{-1}. In Figure 4b–d, light-emitting diode (LED)-liquid alloy circuits were conformably printed on a serpentine iron foil surface that coated with a thin layer of PDMS, on a parallelly waved paper cup surface and on a radially wrinkled PDMS surface, respectively. In Figure 4e, the LED-liquid alloy helix circuits with width of ≈1 mm was conformably printed on a 3D non-deployed surface of an epoxy strawberry mould with sunken pits (≈2–5 mm widths and ≈2–4 mm depth). And in Figure 4f, a liquid alloy antenna was fabricated on a non-deployed surface of a PDMS hemisphere, showing a return loss of −36 dB at 2.25 GHz. Moreover, we demonstrated the CAD-mask printing process on morphing objects and the fabricated dynamic liquid alloy circuits. As shown in Figure 4g,h and Video S1 (Supporting Information), when targeting on a beating heart made of silicone rubber (Ecoflex 0030), the cPDMS mask could be conformably attached

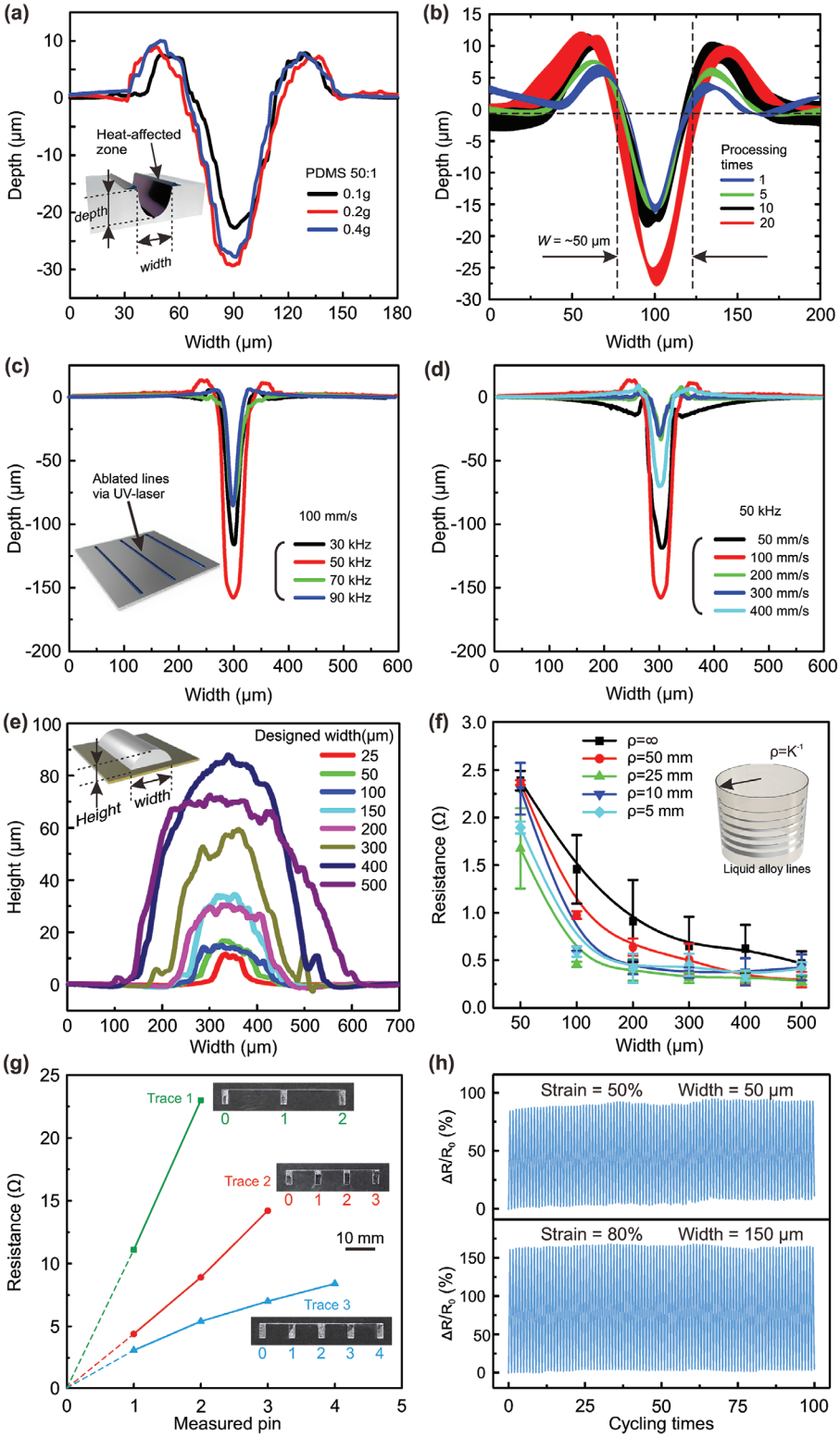

Figure 3. Investigations of laser-ablated patterns and printed liquid alloy traces. a) The cross profiles of laser-ablated grooves of CAD-masks doped with 0.1, 0.2, and 0.4 g carbon black. The masks were treated with parameters of 100 mm s^{-1} and 50 kHz. b) The cross profiles of laser-ablated grooves under different processing times with parameters of 100 mm s^{-1} and 50 kHz. c,d) The cross profiles of laser-ablated grooves based on different pulse repeated frequency c) and laser scanning speed d). e) The cross profile of printed liquid alloy traces with different designed widths on planar surface. f) Measured resistances of printed liquid alloy traces with different widths on curve surface with different curvatures. g) Measured resistance on different pins of printed liquid alloy traces with designed width of 100 μm (experimental width of ≈130 μm). h) Variable resistance of liquid alloy traces with experimental widths of ≈50 and ≈150 μm during stretching-releasing test under 50% and 80% strain, respectively.

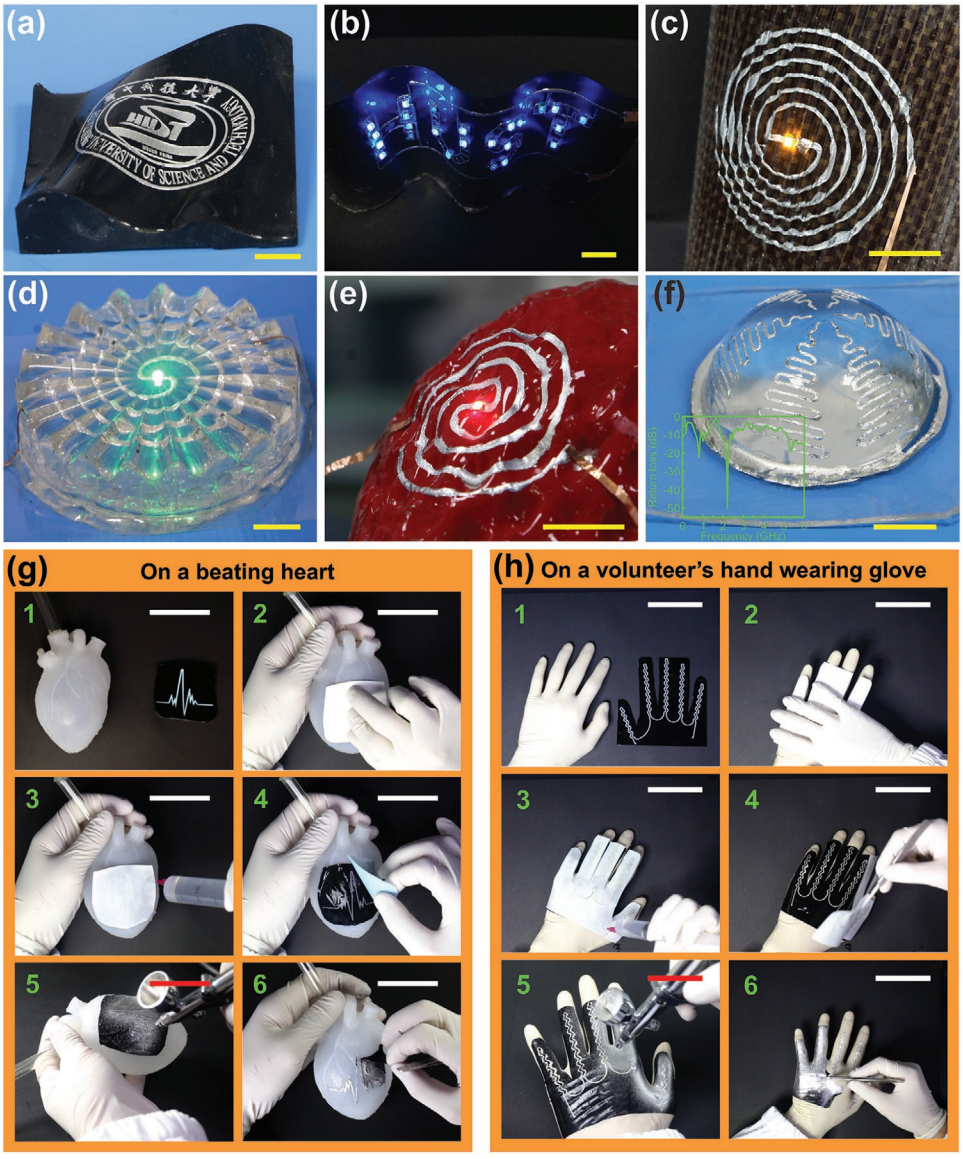

Figure 4. Demonstration of printed conformal liquid alloy circuits on various 3D complex surfaces. a) The liquid alloy pattern of HUST's badge on a 3D carbon black-doped polydimethylsiloxane (cPDMS) surface. b) A blue light-emitting diodes (LEDs)-liquid alloy circuit with shape of "HUST" printed on a waved iron substrate coated with a thin layer of PDMS. c) A yellow LED-liquid alloy helix circuit on a parallelly wrinkled paper cup surface. d) A green LED-liquid alloy helix circuit conformably printed on a radially wrinkled PDMS surface. e) A red LED-liquid alloy helix circuit conformably printed on a complex strawberry mould surface with irregular pits. f) An antenna on a PDMS semi-spherical surface, the inset shows the measure return loss of the antenna. g) The CAD-mask printing process on a beating elastomeric heart. h) The CAD-mask printing process on a volunteer's hand wearing a natural rubber glove. Scale bars = 10 mm.

on the 3D surface of the elastomeric heart during deforming process. In addition, we also conducted the CAD-mask printing process on a volunteer's hand wearing a natural rubber glove. These results reveal that the printing method can be used for fabricating functional circuits on both static and dynamic materials' surfaces with sophisticated topographies.

2.4. Demonstrations

For better exploring the potential usage of CAD-mask printing in practical applications, first, two liquid alloy circuits were conformably printed on both sides of a wheel with good compliance and attachability to work as tactile sensors (**Figure 5**a). After being encapsulated, the integrated sensors can detect the gripping statuses of human hand on the wheel with good robustness and reliability (Figure 5b,c, Video S2, Supporting Information). Then, the wheel connected with a feedback circuit was mounted on a car (Figure 5d). During driving, as shown in Figure 5e and Video S2 (Supporting Information), the variable capacitance reflects the safety driving modes (hand gripping on the wheel, the blue areas), and the operational modes that provides the driver a short time to do necessary operations, e.g., hand relax or indicator switch (hand off the wheel, the yellow

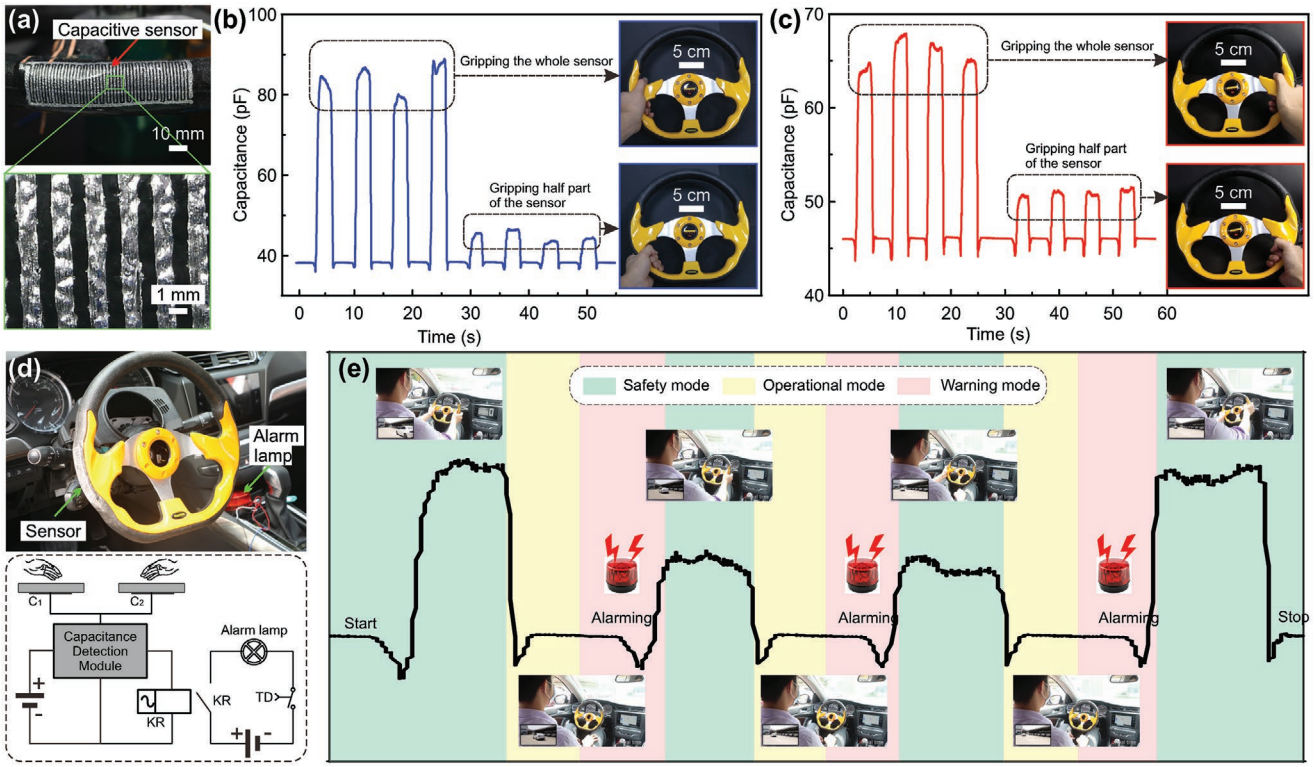

Figure 5. Demonstration of conformal liquid alloy capacitive sensor for driving detection. a) The liquid alloy circuit conformably printed on the surface of a polyurethane wheel and its zoomed-in texture. b,c) Variable capacitance on condition of gripping the whole sensor and gripping half part of the sensor, when using left hand and right hand, respectively. d) The mounted driving mode detecting circuit and its logic illustration. e) The real driving detection including safety mode, operational mode, and warning mode.

areas, and here, we set in as 5 s), and if the operational time exceeds 5 s, it would turn into the warning mode with lamp alarming and buzzing to remind the driver of risk.

To extend the applicability of our CAD-mask printing, we combined the thermo-chromic inks with liquid alloy CAD-mask printing, to configure an anthropomorphic social robot with color change feature, **Figure 6**. After being integrated on a hand and a face model, the capacitive and resistive sensors played the role of detecting and heating modules, respectively. As shown in Figure 6a, the variable capacitance could be used as a trigger for stimulate the heating of sensor on the face. By combining with CAD-mask printing thermochromic inks (Figure S9, Supporting Information), the face could turn red when being heated up to ≈30 °C (Figure 6b). Therefore, the anthropomorphic functional layer was integrated on the inanimate face model, as shown in Figure 6c and Video S3 (Supporting Information), when touching the hand, the resistive circuit started to be heated and the face turned into red, showing a "nervous and shy" state that was similar to human face. The result suggests that our method is potential for fabricating social robots and endowing them with more abilities.

To visually demonstrate the dynamic compliant liquid alloy circuits fabricated by CAD-mask printing, as shown in **Figure 7**a and Video S1 (Supporting Information), after atomized spraying and peeling off the mask, the liquid alloy circuit shows a periodic variable resistance with the period of heart beating, indicating a good dynamic and compliance. In addition, in Figure 7b, both CAD-mask and the printed liquid alloy circuit showed an excellent compliance and robustness, which helped detect several gestures via the variable resistance. We also demonstrated compliant liquid alloy circuits with smaller width (designed width of 50 μm, experimental width of ≈99.3–314.6 μm) on the beating elastomeric heart (Figure S10, Supporting Information). These results reveal that our printing process is not only suitable for static substrates with 3D complex topographies, but is also potential for morphing objects with dynamic surfaces or shapes.

3. Conclusions

Briefly, by employing an ultra-soft and stretchable cPDMS film under UV-laser patterning, we can fabricate a conformal, attachable, and dynamic mask to seamlessly cover on diverse materials with 3D complex static even dynamic morphologies/shapes. Combining with atomized spraying, the liquid alloy circuits can be conformably printed not only on static surfaces but also on dynamic objects with good compliance and robustness. The driving modes detecting wheel and color change face model reveal the application potential of our CAD-mask printing technique on fabricating functional layers of 3D morphing electronics and robotics. Most importantly, the dynamically conformal printing process provides an effective way to real-time fabricating dynamic compliant liquid alloy circuits on morphing objects such as soft robots, living organs/creatures and endorses them interesting features/functions.

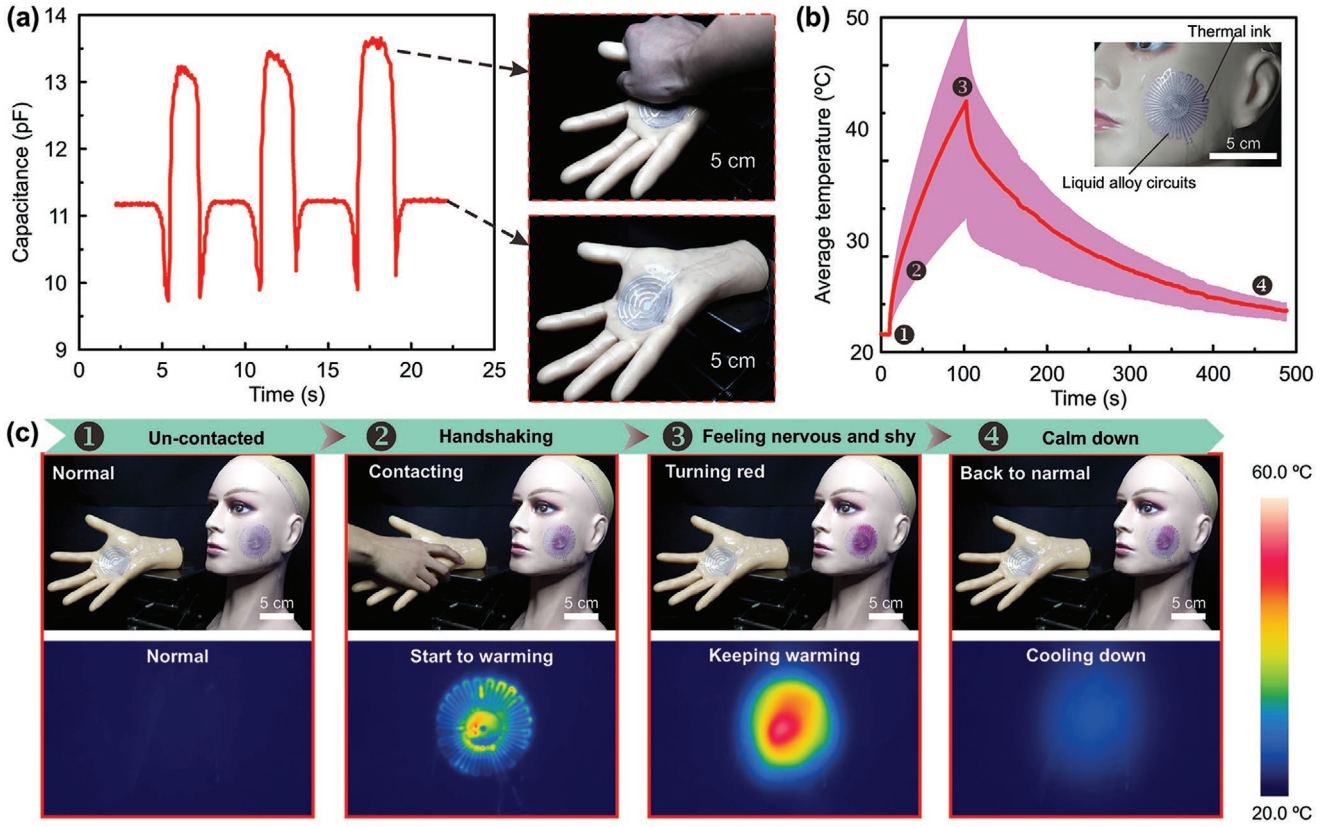

Figure 6. Demonstration of conformal liquid alloy circuits on anthropomorphic model. a) Characterization of the liquid alloy receptor that conformably attached on a hand model. b) The average temperature of the liquid alloy heating circuit that attached on a face model. c) A simulated social reaction of a model with conformal liquid alloy circuits and thermal ink.

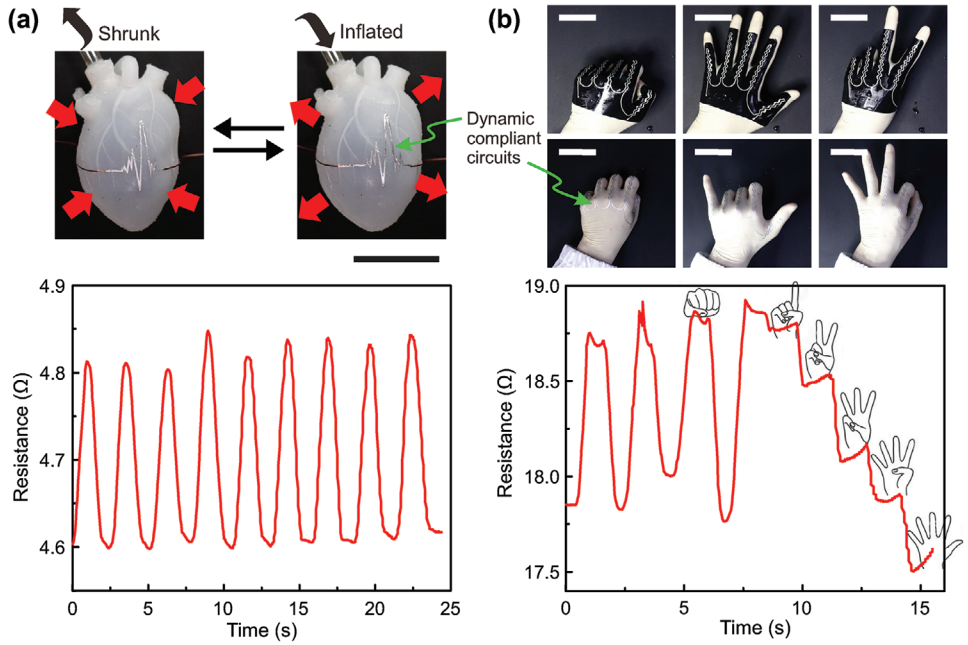

Figure 7. Demonstrations of printed dynamic compliant liquid alloy circuits on morphing surfaces via CAD-masks. a) The shrunk and inflated states of the elastomeric heart, and corresponding variable resistance on dynamic liquid alloy circuit. b) Conformability and attachability characterization of CAD-mask and liquid alloy circuit under different gestures; corresponding variable resistance. Scale bars = 5 mm.

4. Experimental Section

CAD-Mask Preparation: The CAD-mask was prepared by mixing PDMS (Sylgard 184, Dow Corning Corporation, USA) and carbon black (XC72R, Carbot, Alibaba, China). The silicone base and carbon black were stirred manually with a glass rod for ≈3 min and then by digital stirring (RW 20, IKA, Germany) at ≈2000 rpm for ≈3 min. After being cooled down for ≈5 min, the mixture was then mixed with the curing agent manually with the glass rod for 3 min. After being vacuumed to remove bubbles, the mixture was spread on a toner transfer paper (Pulsa professional fx) via a film applicator (PA2041, BYK, Wesel, Germany). Then, the cPDMS film was cured at 75 °C for 45 min in an oven (UF 55 plus, Memmert, Gernamy). Finally, the cPDMS film was selectively patterned using a UV laser marker (HGL-LSU3/5EI, Huagong Laser, Wuhan, China) with a pulse width of 0.10 µs and a working current of 33.5 A. And a CAD-mask was obtained after removing the residua with a tweezer.

Printing Process: The liquid alloy (Galinstan, Geratherm Medical AG, Geschwenda, Germany) was sprayed using a spaying gun ((Infinity CRplus 0.4, Harder und Steenbeck, Norderstedt, Germany) that connected with Nitrogen (N_2, 99.9% purity) and a precision pressure regular (ML-500XII, Musashi, Japan). The CAD-mask printing was recorded by a digital camera (Canon EOS 70D, Tokyo, Japan).

Characterization: The elastomer sample for tensile test was cut into a dumbbell shape with size of 4 × 75 mm by a cutoff knife (Kunshan Creator Testing Instrument Co. Ltd., China). The tensile test was conducted with a universal tensile instrument (5944, Instron, Boston, USA) to obtain the stress and strain. The bending stiffness was calculated by $Et^3/12(1-\nu^2)$, where E is the Young's modulus, t is the thickness, and ν is the Poisson ratio of the material. Noted that the t and ν were 100 µm and 0.49 in this work, respectively.

The energyrelease rate measurement setup was based on aninternational standard test method for 90° peelingresistance of energy release rate (Designation:ASTM D 6862-2004) and test method for peelingstrength of pressure-sensitive tape (Designation:GB/T 2792-1981). The adhesion force was conducted with a homemade measurement setup of a force transducer (Alibaba, China) at a peeling speed of 100 mm s^{-1} as shown in Figure S3 (Supporting Information). A 50 µm thick of the sample was spread and cured on a PET film (50 µm thickness) and then, cut into a size of 150 × 20 mm. After the sample was laminated on the testing surface, a roller was employed to ensure the attachment tightly and evenly before peeling test. The energy release rate (G) is defined as $G = F/w$, where the F refers to adhesion force and the w refers to the width of samples for peeling test.

The cross profiles of laser-ablated grooves and printed liquid alloy circuits were observed with an ultra-depth 3D microscope (DSX 510, Olympus, Tokyo, Japan) and a laser scanning confocal microscope (VK-X200K, Keyence, Osaka, Japan). The variable resistance and capacitance of sensors were measured with a digital multimeter (34461A, Keysight Technologies, Shanghai, China) and a precision LCR meter (E4980AL, Keysight, Shanghai, China). The return loss of the antenna was measured by a FieldFox handheld RF analyzer (N9914A, Keysight Technologies, Shanghai, China).

Demonstrations: The strawberry model was supplied by a commercial 3D printing company (WeNext Technology Co. Ltd., Shenzhen, China). The beating Ecoflex 0030 (Smooth-on Inc, Easton, USA) heart was casted with an epoxy-based heart mould (WeNext Technology Co. Ltd., Shenzhen, China), and inflated by a syringe connected with a peristaltic pump (purchased from Alibaba, China). The steering wheel (purchased from Alibaba, China) was seamlessly integrated with capacitive sensors and encapsulated with PDMS as illustrated in Figure S9a (Supporting Information). A motor car's original steering wheel was replaced by our circuits-integrated one. And after being mounted with the feedback circuit (a relay, a delay module, a switch module, and an alarm lamp, all of them were purchased from Alibaba, China), the testing car was employed for driving modes detection. The hand and face model (purchased from Alibaba, China) in Figure 6 were coated with a thin layer PDMS and encapsulated with Ecoflex 0030. The thermos-chromic inks were purchased from Alibaba, China. And the real-time temperature field was recorded by a thermal imaging camera (FLIR T630sc, FLIR system, Flir Systems AB, Täby, Sweden).

All experiments complied with the guidelines by Huazhong University of Science and Technology. All subjects were volunteers (co-authors of the work) and provided informed consent.

Supporting Information

Supporting Information is available from the Wiley Online Library or from the author.

Acknowledgements

S.Z. and J.J. contributed equally to this work. This work was supported by the National Natural Science Foundation of China (U1613204) and the Guangdong Innovative and Entrepreneurial Research Team Program (2016ZT06G587). The general characterization facilities are partly provided by the Flexible Electronics Manufacturing Laboratory in Comprehensive Experiment Center for Advanced Manufacturing Equipment and Technology at Huazhong University of Science and Technology.

Conflict of Interest

The authors declare no conflict of interest.

Data Availability Statement

Research data are not shared.

Keywords

attachable and dynamic mask, compliant liquid alloy circuits, conformal, deformable morphology, dynamically conformal printing

Received: December 21, 2020
Revised: March 11, 2021
Published online:

[1] D.-H. Kim, N. Lu, R. Ma, Y.-S. Kim, R.-H. Kim, S. Wang, J. Wu, S. M. Won, H. Tao, A. Islam, K. J. Yu, T.-i. Kim, R. Chowdhury, M. Ying, L. Xu, M. Li, H.-J. Chung, H. Keum, M. McCormick, P. Liu, Y.-W. Zhang, F. G. Omenetto, Y. Huang, T. Coleman, J. A. Rogers, *Science* **2011**, *333*, 838.

[2] a) J. Deng, H. Yuk, J. Wu, C. E. Varela, X. Chen, E. T. Roche, C. F. Guo, X. Zhao, *Nat. Mater.* **2021**, *20*, 229; b) J. Viventi, D.-H. Kim, J. D. Moss, Y.-S. Kim, J. A. Blanco, N. Annetta, A. Hicks, J. Xiao, Y. Huang, D. J. Callans, J. A. Rogers, B. Litt, *Sci. Transl. Med.* **2010**, *2*, 24ra22; c) C. Dagdeviren, Y. Shi, P. Joe, R. Ghaffari, G. Balooch, K. Usgaonkar, O. Gur, P. L. Tran, J. R. Crosby, M. Meyer, Y. Su, R. Chad Webb, A. S. Tedesco, M. J. Slepian, Y. Huang, J. A. Rogers, *Nat. Mater.* **2015**, *14*, 728; d) H. Lee, T. K. Choi, Y. B. Lee, H. R. Cho, R. Ghaffari, L. Wang, H. J. Choi, T. D. Chung, N. Lu, T. Hyeon, *Nat. Nanotechnol.* **2016**, *11*, 566.

[3] a) N. Lu, D.-H. Kim, *Soft Rob.* **2013**, *1*, 53; b) K. K. Rebecca, presented at Proc.SPIE **2015**; c) C. M. Boutry, M. Negre, M. Jorda, O. Vardoulis, A. Chortos, O. Khatib, Z. Bao, *Sci. Rob.* **2018**, *3*, eaau6914.

[4] a) J. A. Fan, W.-H. Yeo, Y. Su, Y. Hattori, W. Lee, S.-Y. Jung, Y. Zhang, Z. Liu, H. Cheng, L. Falgout, M. Bajema, T. Coleman, D. Gregoire, R. J. Larsen, Y. Huang, J. A. Rogers, *Nat. Commun.* **2014**, *5*, 3266; b) J. A. Rogers, T. Someya, Y. Huang, *Science* **2010**, *327*, 1603; c) C. Wang, C. Wang, Z. Huang, S. Xu, *Adv. Mater.* **2018**, *30*, 1801368; d) M. L. Hammock, A. Chortos, B. C. K. Tee, J. B. H. Tok, Z. Bao, *Adv. Mater.* **2013**, *25*, 5997.
[5] L. Wang, N. Lu, *J. Appl. Mech.* **2016**, *83*, 041007.
[6] a) P. Peng, K. Wu, L. Lv, C. F. Guo, Z. Wu, *Adv. Mater. Technol.* **2018**, *3*, 1700264; b) S. Yang, Y.-C. Chen, L. Nicolini, P. Pasupathy, J. Sacks, B. Su, R. Yang, D. Sanchez, Y.-F. Chang, P. Wang, D. Schnyer, D. Neikirk, N. Lu, *Adv. Mater.* **2015**, *27*, 6423.
[7] a) J. T. Muth, D. M. Vogt, R. L. Truby, Y. Mengüç, D. B. Kolesky, R. J. Wood, J. A. Lewis, *Adv. Mater.* **2014**, *26*, 6307; b) T. J. Wallin, J. Pikul, R. F. Shepherd, *Nat. Rev. Mater.* **2018**, *3*, 84; c) J. J. Adams, E. B. Duoss, T. F. Malkowski, M. J. Motala, B. Y. Ahn, R. G. Nuzzo, J. T. Bernhard, J. A. Lewis, *Adv. Mater.* **2011**, *23*, 1335; d) L. W. T. Ng, X. Zhu, G. Hu, N. Macadam, D. Um, T.-C. Wu, F. Le Moal, C. Jones, T. Hasan, *Adv. Funct. Mater.* **2019**, *29*, 1807933.
[8] a) Y. Wang, L. Yin, Y. Bai, S. Liu, L. Wang, Y. Zhou, C. Hou, Z. Yang, H. Wu, J. Ma, Y. Shen, P. Deng, S. Zhang, T. Duan, Z. Li, J. Ren, L. Xiao, Z. Yin, N. Lu, Y. Huang, *Sci. Adv.* **2020**, *6*, eabd0996; b) A. Carlson, A. M. Bowen, Y. Huang, R. G. Nuzzo, J. A. Rogers, *Adv. Mater.* **2012**, *24*, 5284.
[9] a) H. Chang, R. Guo, Z. Sun, H. Wang, Y. Hou, Q. Wang, W. Rao, J. Liu, *Adv. Mater. Interfaces* **2018**, *5*, 1800571; b) U. Daalkhaijav, O. D. Yirmibesoglu, S. Walker, Y. Mengüç, *Adv. Mater. Technol.* **2018**, *3*, 1700351.
[10] Y. Liu, J. Li, S. Song, J. Kang, Y. Tsao, S. Chen, V. Mottini, K. McConnell, W. Xu, Y.-Q. Zheng, J. B. H. Tok, P. M. George, Z. Bao, *Nat. Biotechnol.* **2020**, *38*, 1031.
[11] a) M. D. Dickey, *Adv. Mater.* **2017**, *29*, 1606425; b) X. Wang, J. Liu, *Micromachines* **2016**, *7*, 206.
[12] S. Cheng, A. Rydberg, K. Hjort, Z. Wu, *Appl. Phys. Lett.* **2009**, *94*, 144103.
[13] a) J. W. Boley, E. L. White, G. T. C. Chiu, R. K. Kramer, *Adv. Funct. Mater.* **2014**, *24*, 3501; b) Y. Zheng, Z. He, Y. Gao, J. Liu, *Sci. Rep.* **2013**, *3*, 1786.
[14] A. Tabatabai, A. Fassler, C. Usiak, C. Majidi, *Langmuir* **2013**, *29*, 6194.
[15] R. K. Kramer, C. Majidi, R. J. Wood, *Adv. Funct. Mater.* **2013**, *23*, 5292.
[16] S. H. Jeong, K. Hjort, Z. Wu, *Sci. Rep.* **2015**, *5*, 8419.
[17] Y. Yu, F. Liu, R. Zhang, J. Liu, *Adv. Mater. Technol.* **2017**, *2*, 1700173.
[18] S. Zhang, B. Wang, J. Jiang, K. Wu, C. F. Guo, Z. Wu, *ACS Appl. Mater. Interfaces* **2019**, *11*, 7148.
[19] J. Jiang, S. Zhang, B. Wang, H. Ding, Z. Wu, *Small* **2020**, *16*, 2003833.
[20] a) X. Wang, Y. Zhang, R. Guo, H. Wang, B. Yuan, J. Liu, *J. Micromech. Microeng.* **2018**, *28*, 034003; b) M. Tavakoli, M. H. Malakooti, H. Paisana, Y. Ohm, D. Green Marques, P. Alhais Lopes, A. P. Piedade, A. T. de Almeida, C. Majidi, *Adv. Mater.* **2018**, *30*, 1801852.
[21] a) A. F. Silva, H. Paisana, T. Fernandes, J. Góis, A. Serra, J. F. J. Coelho, A. T. de Almeida, C. Majidi, M. Tavakoli, *Adv. Mater. Technol.* **2020**, *5*, 2000343; b) R. Guo, J. Tang, S. Dong, J. Lin, H. Wang, J. Liu, W. Rao, *Adv. Mater. Technol.* **2018**, *3*, 1800265.
[22] G. Saada, M. Layani, A. Chernevousky, S. Magdassi, *Adv. Mater. Technol.* **2017**, *2*, 1600289.
[23] P. A. Lopes, H. Paisana, A. T. De Almeida, C. Majidi, M. Tavakoli, *ACS Appl. Mater. Interfaces* **2018**, *10*, 38760.
[24] a) H. Gui, S. Tan, Q. Wang, Y. Yu, F. Liu, J. Lin, J. Liu, *Sci. China: Technol. Sci.* **2017**, *60*, 306; b) Y. Y. Yao, Y. J. Ding, H. P. Li, S. Chen, R. Guo, J. Liu, *Adv. Eng. Mater.* **2019**, *21*, 1801363; c) H. Chang, P. Zhang, R. Guo, Y. Cui, Y. Hou, Z. Sun, W. Rao, *ACS Appl. Mater. Interfaces* **2020**, *12*, 14125.
[25] a) S. H. Jeong, K. Hjort, Z. Wu, *Sci. Rep.* **2015**, *5*, 8419; b) B. Wang, K. Wu, K. Hjort, C. Guo, Z. Wu, *Soft Rob.* **2019**, *6*, 414.
[26] a) M. P. Wolf, G. B. Salieb-Beugelaar, P. Hunziker, *Prog. Polym. Sci.* **2018**, *83*, 97; b) S. H. Jeong, S. Zhang, K. Hjort, J. Hilborn, Z. Wu, *Adv. Mater.* **2016**, *28*, 5830.
[27] S. Zhang, Q. Jiang, Y. Xu, C. F. Guo, Z. Wu, *Micromachines* **2020**, *11*, 682.